JOURNAL OF APPLIED PHYSICS VOLUME 96, NUMBER 9 1 NOVEMBER 2004

A physically based model for the spatial and temporal evolution of self-interstitial agglomerates in ion-implanted silicon

Christophe J. Ortiz,[a] Peter Pichler, and Tim Fühner
Fraunhofer Institute Integrated Systems and Device Technology, 91058 Erlangen, Germany

Filadelfo Cristiano
LAAS/CNRS, 31077 Toulouse Cedex, France

Benjamin Colombeau and Nicholas E. B. Cowern
Advanced Technology Institute, Universtity of Surrey, Guildford GU2 7XH, United Kingdom

Alain Claverie
CEMES/CNRS, 31055 Toulouse Cedex, France

(Received 13 May 2004; accepted 30 June 2004)

A physically motivated model that accounts for the spatial and temporal evolution of self-interstitial agglomerates in ion-implanted Si is presented. For the calibration of the model, a genetic algorithm is used to find the optimum set of physical parameters from experimental data. Mean-size evolution of {113} defects obtained by transmission electron microscopy and self-interstitial oversaturation results measured in the vicinity of extended defects are combined in the same fitting procedure. The calibration of parameters shows that binding energies of small self-interstitial clusters exhibit strong maxima, as reported in other investigations. Results of the calibrated model are compared to experimental data obtained in complementary investigations. It is demonstrated that the model is able to predict a wide variety of physical phenomena, from the oversaturation of self-interstitials via the mean-size evolution of {113} defects to the depth distribution of the density of the latter. © *2004 American Institute of Physics*. [DOI: 10.1063/1.1786678]

I. INTRODUCTION

Because of its supreme reproducibility and the rather easy restriction to local areas by masking, doping by the implantation of ions will remain the method of choice for the next technology generations. Its major disadvantage in the miniaturization race results from its nonconservative nature. The extra atoms introduced are well known to generate excess self-interstitials, which lead to the so-called transient enhanced diffusion (TED) of dopants during postimplantation treatments required to anneal the implantation damage. The duration and amplitude of this TED have been shown to be strongly linked to the thermal behavior of extrinsic defects such as dislocation loops,[1] {113} defects,[2,3] and, more recently, small self-interstitial clusters.[4] Therefore, a considerable effort has been devoted to the understanding of physical mechanisms controlling their nucleation, growth, and dissolution in order to provide models[4–8] that are sufficiently predictive to support design and optimization of devices in leading-edge technologies. However, some of the previous models[4,5] were based on the assumption that extended defects only form at the position of maximum implantation damage. This assumption severely restricts the models to the prediction of the mean self-interstitial oversaturation centered at the defects and does not account for the spatial variation of the defect distribution. Other models, such as the one presented in Ref. 6, describe the size distribution of defects in terms of moments and are based on the assumption that the distribution is the one that minimizes the free energy of the system. On the other hand, although models proposed in Refs. 7 and 8 describe the full-size distribution of defects and take into account the spatial variation of defect density, they assume that all defects have the geometry and properties of {113} defects, even clusters of few atoms. In this work, we propose a fully calibrated model that describes the temporal and spatial evolution of extended defect distribution—small self-interstitial clusters and {113} defects—and which accounts for recent experimental observations. In the first section of the paper we present a general formulation of our kinetic model. The next part of the paper is dedicated to the calculation of rate constants of the model. In the last section, we present the optimization procedure for extraction of the free physical parameters of the model from experimental data. The values found are discussed and compared to those found in the literature. In order to test the validity of our physically based model as well as the consistency of the extracted parameters, the calibrated model is used to simulate various types of experimental data found in complementary investigations. It will be shown that our one-dimensional implementation of the model is able to describe quantitatively the oversaturation of self-interstitials as well as major {113}-defect-related phenomena such as the depth dependence of their distribution characterized recently.

II. FORMULATION OF THE MODEL

Since there were various partly incompletely described and ill-motivated formulations for the agglomeration of self-interstitials introduced in the literature, we will first derive

[a]Author to whom correspondence should be addressed; electronic mail: christophe.ortiz@iisb.fraunhofer.de

 © 2004 American Institute of Physics

and motivate a general formulation. The basis of our approach is a system of continuity equations for the mobile self-interstitials and the extended defects which describes the kinetics of the system. Thereafter, the interactions of self-interstitials with the surface will be considered which leads directly to their boundary conditions. Finally, the initial conditions for self-interstitials and defects will be discussed.

A. Continuity equations

As extrinsic defects are precipitates of silicon atoms, we can adopt the classical theory of nucleation[9] to describe their formation and evolution from a self-interstitial oversaturation. According to this theory, we assume that extended defects form by agglomeration of mobile self-interstitials through binary reactions of the type

$$I_n + I \underset{k_{n+1}^-}{\overset{k_n^+}{\rightleftarrows}} I_{n+1}, \tag{1}$$

where I_n and I_{n+1} denote defects comprising n and $n+1$ Si atoms, respectively. In this work we assume that the I_n are immobile while self-interstitials, denoted by the symbol I, are mobile. The forward rate constant k_n^+ represents the ability of defects of n atoms to capture self-interstitials while k_{n+1}^- is the emission rate constant of self-interstitials, i.e., the frequency at which Si atoms dissociate from a defect containing $n+1$ atoms. Expressions for these two coefficients will be derived in the following section.

In order to predict the evolution of free self-interstitials I, their reactions with defects of all possible sizes (1) and also their diffusion have to be taken into account. In the following, we only consider situations in which the oversaturation of self-interstitials is very high. Then, vacancies play only a minor role and can be neglected for the sake of simplicity. However, we consider that the initial dose of self-interstitials is low enough so that the volume fraction of extended defects is small. As a consequence, the distance between extended defects is such that diffusional fields around defects do not overlap (mean-field approximation). In this approximation, the mean concentration C_I of self-interstitials between defects is governed by the following partial differential equation:

$$\frac{\partial C_I}{\partial t} = D_I \frac{\partial^2 C_I}{\partial x^2} - 2k_1^+ C_I^2 + 2k_2^- C_{I_2} - \sum_{n=2}^{N_{\max}} (k_n^+ C_{I_n} C_I - k_{n+1}^- C_{I_{n+1}}). \tag{2}$$

Since we consider in the following only experiments with intrinsically doped samples, D_I, the diffusion coefficient of self-interstitials in silicon, will depend only on temperature. $N_{\max}$ is the largest possible size of defects in the system. The first term on the right-hand side (RHS) of Eq. (2) describes the diffusion of self-interstitials. The two next terms arise from the formation and dissociation of di-interstitial clusters while the sum over n—the last term of the RHS—is the generation-recombination term due to capture and emission of interstitials by/from defects of size $n \geqslant 2$. In the region where defect formation can be neglected, all but the first term of the RHS vanish and Eq. (2) reduces to the well-known Fick's second law.

Also, according to Eq. (1), it is clear that the concentration C_{I_n} of defects I_n with a discrete number of atoms n ($n \geqslant 2$) follows a Markovian process.[10] Thus, the evolution of C_{I_n}, at a given depth x, changes according to the Master equation

$$\frac{\partial C_{I_n}}{\partial t} = k_{n-1}^+ C_{I_{n-1}} C_I - k_n^+ C_{I_n} C_I - k_n^- C_{I_n} + k_{n+1}^- C_{I_{n+1}}. \tag{3}$$

Although depth does not explicitly appear in Eq. (3), we must emphasize that the concentration C_{I_n} of defects of size n will, in general, vary with depth. Indeed, the rate at which defects of size n evolve depends on the local concentration C_I of interstitials, which is depth dependent according to Eq. (2). Moreover, in practice, the initial self-interstitial oversaturation that is produced during ion implantation is not uniform and extends from the surface up to a certain depth. Therefore, the concentration of extended defects must be calculated not only at the position of maximum damage, in contrast to other works,[4,5] but over the whole depth. As it will be discussed later in this work, we will see that this is important to reproduce recent experimental observations obtained by Colombeau *et al.*[11] on the time evolution of the spatial distribution of the {113}-defect density. Thus, our model takes into account the temporal and spatial evolution of the extended-defect band.

B. Boundary conditions for self-interstitials: Recombination at the surface

In addition to the diffusion and reaction of self-interstitials with defects, one must also take their interaction with the silicon surface into account, which is generally considered as a strong sink[4,12] for intrinsic point defects (I, V). In order to model the recombination of interstitials at the surface, we used first-order boundary conditions,[13] assuming that the flux of interstitials is proportional to the excess of point defects and that the annihilation of self-interstitials at kinks is diffusion limited.[14] The flux of interstitials at the surface is thus given by the following equation:

$$J_I(x=0) = -\frac{D_I}{\lambda}[C_I(x=0) - C_I^{eq}], \tag{4}$$

where $J_I(x=0)$ is the interstitial flux at the surface, $C_I(x=0)$ the concentration of interstitials at the boundary, C_I^{eq} the thermodynamic equilibrium concentration of self-interstitials, and λ the surface-recombination length. λ appears as a fictitious distance above the surface at which the concentration of self-interstitials is at equilibrium. This is schematically represented in Fig. 1. Cowern *et al.*[15] estimated the recombination length of interstitials to be lower than 5 nm at 900 °C and 1000 °C under N_2. To test the influence of this parameter, simulations were performed with different values of the recombination length ($\lambda < 10$ nm). No differences in the results were observed since the mean depth of the extended defects was considerably larger than λ in the experiments used for calibration and validation. Therefore, in the

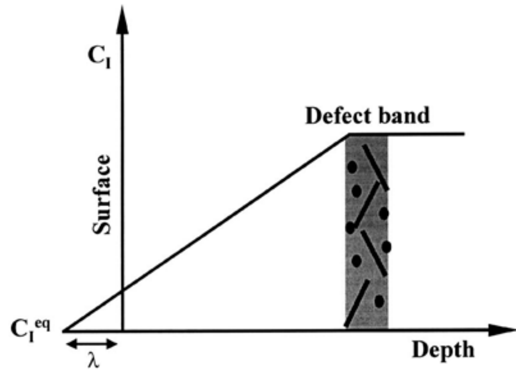

FIG. 1. Schematic definition of the recombination length.

following, we shall assume a value of 5 nm for the recombination length of self-interstitials.

C. Initial conditions

As initial conditions for self-interstitials, we used the so-called "+1" model,[16] which assumes that *I-V* recombination occurs instantaneously at the beginning of the annealing. According to this model, excess interstitials are generated only by the incorporation of the implanted species on substitutional sites and the dose of interstitials is roughly equal to the implanted dose. This picture is consistent with several experimental findings[2,17] showing that, for subamorphizing Si^+ implants, the areal density of interstitials bound by {113} defects after short anneals is roughly equal to the Si implantation dose. Therefore, the +1 model holds here and we can assume that the surplus of silicon atoms from the implantation remains as self-interstitial profile. The Si profile after implantation was calculated using TRIM.[18] In addition, we assumed that all the excess self-interstitials created by the ion-implantation step are free to diffuse and that no self-interstitial complexes are formed at $t=0$. We are aware of the fact that intrinsic point defects are highly mobile at room temperature[19–21] so that it is likely that they will form complexes already before annealing. For example, in their investigation, Cowern *et al.*[4] adopted the +1 model and assumed that all clusters are initially of size $n=2$, i.e., di-interstitials. We tested this assumption for several anneal conditions but no differences compared to the assumption made above were observed in the simulation results. To solve the set of partial differential equations, (PDE), Eqs. (2) and (3), with the boundary conditions described by Eq. (4), we used the PDE solver PROMIS1.5.[22]

III. CAPTURE AND EMISSION RATE CONSTANTS

As we can see from Eqs. (2) and (3) defined in the preceding section, the growth rate of extended defects depends on the rate at which they capture and emit free interstitials. As the self-interstitial supersaturation is at the origin of TED of dopants in submicron devices, it is therefore crucial to properly estimate the capture and emission rate constants defined in Eq. (1), namely, k_n^+ and k_{n+1}^-. This section is organized as follows. First, regardless of the defect type, we shall show that the absorption and emission rate constants of interstitials depend on two essential characteristics of the defects, their effective capture radius and their differential formation energy, which are geometry and size dependent. Then, as small silicon clusters and {113} defects may coexist with different geometries, we shall give an expression of the effective capture radius for each type of defect. Finally, the last part of this section will be dedicated to the calculation of the differential formation energy of these two types of extended defects, which, as it will be shown, reflects the magnitude of the TED and is thus a main parameter in the modeling of the evolution of extended defects.

A. Capture rate constant

In this work, the incorporation of mobile species—self-interstitials—to extended defects is assumed to be only diffusion limited, i.e., there is no energy barrier in excess of the migration energy of interstitials at the precipitate/silicon interface. Also, as extended defects may adopt different geometries, the absorption rate constant must reflect their capture area as well as the radial extension of the diffusion field around the defect. According to this, we can write a general expression for the absorption rate constant:

$$k_n^+ = \frac{A_n}{R_{eff}} D_I. \tag{5}$$

where A_n is the capture area of an extended defect containing n atoms and R_{eff} the effective radial extension of the diffusion field around it. The ratio A_n/R_{eff} is an important characteristics of the defect as it depends on its size and geometry. A related parameter,

$$a_n = \frac{1}{4\pi} \frac{A_n}{R_{eff}}, \tag{6}$$

is also called sometimes the effective capture radius of the defect in the literature.

B. Emission rate constant

Having quantified the absorption rate constant k_n^+, we need to derive also the emission rate constant k_{n+1}^-. To do so, we use the fact that, in steady state, absorption and emission rates must be equal. Then, writing the so-called law of mass action for Eq. (1) in steady state and expressing the concentration in terms of site fractions x, we obtain

$$k_{n+1}^- = k_n^+ \left(\frac{C_{I_n} C_I}{C_{I_{n+1}}} \right)_{steady\ state} = k_n^+ C_{\mathrm{Si}} \left(\frac{x_{I_n} x_I}{x_{I_{n+1}}} \right)_{steady\ state}. \tag{7}$$

Here C_{Si} is the concentration of Si sites ($\approx 5 \times 10^{22}$ cm^{-3}). To derive the equation above we have assumed that the number of available sites for point and extended defects are the same and equal to C_{Si}. Indeed, the possible deviations of the numbers of sites for the reactants from the number of lattice sites are on the order of unity.

On the other hand, the law of mass action can also be written in terms of energetics of defects as follows:

$$\frac{x_{I_n} x_I}{x_{I_{n+1}}} = \frac{\theta_{I_n} \theta_I}{\theta_{I_{n+1}}} \exp\left(-\frac{G^f_{I_n} + G^f_I - G^f_{I_{n+1}}}{k_B \cdot T}\right). \tag{8}$$

where k_B is the Boltzmann constant and T the absolute temperature. G^f_I is the Gibbs free energy of formation of a self-interstitial in the undisturbed Si lattice. Similarly, $G^f_{I_n}$ and $G^f_{I_{n+1}}$ are the Gibbs formation energies of defects of sizes n and $n+1$, respectively. $G_B(n) = G^f_{I_n} + G^f_I - G^f_{I_{n+1}}$ is the binding energy with which the last self-interstitial added binds to the extended defect. In Eq. (8), the θ_s denote the internal degrees of freedom of defects. Here, we introduce the energy $E^f(n+1) = G^f_{I_{n+1}} - G^f_{I_n}$, which represents by definition the energetic cost to add one extra Si atom to a defect of n atoms. In the following we will refer to it as the differential formation energy of a defect of n atoms. The concentration of self-interstitials in thermal equilibrium C^{eq}_I in the undisturbed lattice can be derived from statistical thermodynamics. It can be easily demonstrated that it is related to G^f_I by the well-known relation

$$C^{eq}_I = C_{\text{Si}} \exp\left(-\frac{G^f_I}{k_B T}\right). \tag{9}$$

Finally, combining Eqs. (7)–(9), the emission rate constant becomes

$$k^-_{n+1} = k^+_n C^{eq}_I \exp\left(+\frac{E^f(n+1)}{k_B \cdot T}\right). \tag{10}$$

It has to be mentioned that to derive the above equation, we have considered that the binding energy is the most important parameter while degrees of freedom in Eq. (8) are on the order of unity. From Eq. (10) it is clear that $E^f(n)$ can be seen as a measure for the relative stability of an extended defect. The higher the differential formation energy of the defect, the faster it will dissolve, maintaining a higher self-interstitial supersaturation in its vicinity. Therefore, $E^f(n)$ is not only an important characteristic of defects but is also an important parameter that determines the amplitude of the transient enhanced diffusion of dopants in silicon.

C. Effective capture radius of defects

As it is apparent from Eq. (5), the rate at which extended defects capture mobile self-interstitials depends of course on the diffusivity of the latter, but also on the effective capture radius of the former. Since this parameter depends on their size and geometry it is important to know the atomic structure of the different types of defects that may form and coexist. For the purpose of this work, we restrict ourselves to situations in which only small self-interstitial clusters and {113} defects will form. Dislocation loops are not considered in the following although an extension would be straightforward in analogy.

D. Small compact clusters

Since, in practice, the smallest defects that transmission electron microscopy (TEM) can resolve are already 2 nm long {113} defects,[23] i.e., defects containing 40 atoms, little is known about the atomic structure of smaller defects. Therefore, some assumptions must be made with respect to the geometry of the latter. As they are small and probably compact clusters of silicon atoms, we can reasonably assume that they are close to spherical, similarly to what is done in other works.[5,24] In this case, their capture area is simply $A_n = 4\pi r_n^2$, where r_n is the geometrical radius of a cluster of n atoms. For this particular geometry with spherical symmetry, the radial extension of the diffusion field around the defect can be easily calculated and is $R_{eff} = r_n$.[25] Thus, in our model, the capture radius of small self-interstitial clusters is simply expressed as

$$\left.\frac{A_n}{\mathrm{R}_{eff}}\right|_{clusters} = 4\pi r_n. \tag{11}$$

It is a well-known expression which was already derived by Waite[26] in the case of diffusion-limited bimolecular reactions.

E. Elongated {113} defects

In their long history, {113} defects were identified as various structures. It is now believed[27] that these defects are agglomerates of ⟨110⟩ oriented rows of Si self-interstitials as suggested already by early researchers.[28,29] After ion implantation and annealing, {113} defects are observed as long, narrow defects, usually named "rodlike defects." They are sandwiched between two reconstructed {113} surfaces without any dangling bonds in the {110} cross section. Thus, further agglomeration of self-interstitial atoms in the ⟨110⟩ direction does not introduce additional dangling bonds. This is also the reason for their peculiar rodlike morphology, elongated because of the favored growth along the ⟨110⟩ direction. However, as it was emphasized by Claverie *et al.*[30] "*It is important to note that our apparent knowledge of the elongated {113} defects heavily relies on the hypothesis that they have the same atomic structure than the planar {113} defects..*" Indeed, the {113} defects observed after ion implantation are too narrow to allow for accurate TEM analysis while planar {113} defects, which are formed during electron irradiation, are wider and of apparently the same overall structure. On the other hand, Eaglesham *et al.*[2] observed elongated {113} defects after the annealing of samples implanted with silicon ions with 40 keV and a dose of 5×10^{13} cm^{-2}. Based on high-resolution TEM (HRTEM) observations, the authors concluded that the mean width of the {113} defects depends only insignificantly on the annealing conditions and is nearly constant (about 4 nm). Measurements carried out on Si-implanted samples by other authors[31] support this observation. Finally, according to Takeda *et al.*,[32] the areal density of interstitials in {113} defects is 5×10^{14} cm^{-2}. Thus, schematically, {113} defects are planar with a rectangular shape and grow primarily in length. Although their geometry is simple, estimating their capture area is far more difficult than in the case of spherical clusters. Gencer and Dunham[6] proposed that capture of self-interstitials occurs only at the tips of these elongated defects. In contrast, as motivated by other works[5,24] and by results obtained by another research team,[33] we assume in this work that self-interstitials can be also captured at the sides of the

defect, too. Indeed, it has recently been shown[33] that sides of {113} defects are tensile regions, where self-interstitials are preferably captured. Since it is generally observed that {113} defects grow primarily in length, this implies that once a self-interstitial is captured at a side of a defect, it is easily transported along the defect to its tips. Thus, the capture area of a {113} defect increases as it grows and is the sum of three terms: (i) two cylinders at the width sides, (ii) two cylinders along the length sides, and (iii) four hemispheres at the corners, as depicted in Fig. 2. For the radial extension of the diffusion field around a {113} defect, we take the expression derived by Gencer and Dunham.[6] The effective capture radius of a {113} defect is then given by the following expression:

$$\left.\frac{A_n}{R_{\mathrm{eff}}}\right|_{\{113\}} = \frac{2\times 2\pi aL + 2\times 2\pi aW + 4\times 2\pi a^2}{\dfrac{\ln[1+\sqrt{1+(2a/W)^2}] - \ln(2a/W) + \ln[1+\sqrt{1+[2(L+a)/W]^2}] - \ln[2(L+a)/W]}{1/a\sqrt{1+(2a/W)^2} + 1/(L+a)\sqrt{1+[2(L+a)/W]^2}}} \tag{12}$$

wherein L and W are the length and the width of the {113} defect, respectively. a denotes the distance between Si atoms on adjacent lattice sites.

F. Transition from small clusters to {113} defects

According to the assumption we made concerning the geometry of small self-interstitial clusters, their morphology is different from that of {113} defects. Hence, they also have a different effective capture radius. Therefore, it is important to know at which size the transition between small clusters and {113} defects occurs, i.e., the size at which the geometry of defects changes. According to TEM measurements,[23] we know that defects containing only 40 atoms have the same atomic structure as {113} defects. This means that the transition from clusters to {113} defects occurs already for a size below 40 atoms. In their investigation on the energetics of self-interstitial clusters in Si, Cowern *et al.*[4] found that the differential formation energy (called formation energy in their work) of large self-interstitial clusters gently tends toward the differential formation energy expected for small {113} defects. This observation showed that defects of more than 20 atoms are similar, at least in terms of their differential formation energy, to the {113} defects. Theoretical calculations carried out by De Souza *et al.*[34] support this idea, too. Using the empirical Ackland potential,[35] the authors found that a dangling-bond-chain configuration is more favorable than a compact hexagonal configuration for sizes beyond eight atoms. Therefore, they concluded that the transition from small compact clusters to {113} defects occurs for a size of eight atoms. Based on these indications and on other investigations,[5,24] we assume in this work that the transition occurs for a size of ten atoms. In other words, all defects that contain less than ten atoms will be considered as small, compact self-interstitial clusters. The overall variation of the effective capture radius A_n/R_{eff} based on this assumption is shown in Fig. 3. The abrupt jump corresponds to the transition from small clusters to elongated {113} defects, i.e., the size at which defects are expected to undergo a structural transformation.

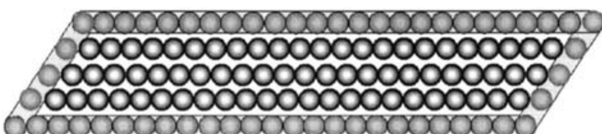

FIG. 2. Schematic representation of a {113} defect and its capture area at the periphery.

G. Energetics of defects

It is now well established that the thermal evolution of extended defects is based on the interchange of mobile self-interstitials between defects of different sizes. During this interchange, defects can either evolve following an Ostwald ripening process, as previously shown by co-workers,[36] or by transforming into another type of defect, arising from the crystallographical reordering of atoms.[37,38] In both cases, the driving force for the evolution of extended defects is the reduction of the total energy of the system, in particular, the reduction of their differential formation energy. As we have seen in a previous section, this latter parameter determines the rate at which defects emit self-interstitials [Eq. (10)]. Since this process determines the oversaturation of self-interstitials during postimplantation anneals, the differential

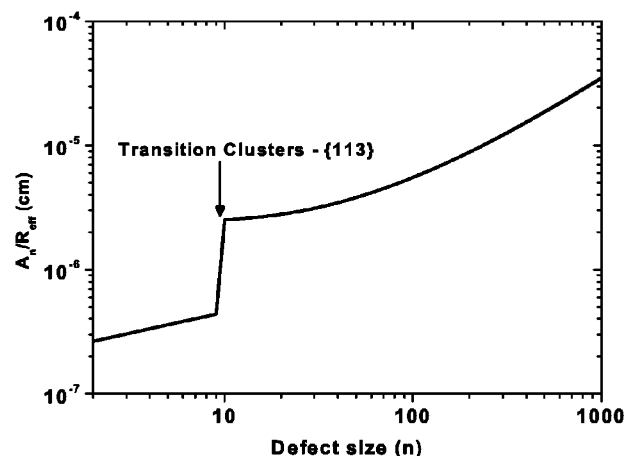

FIG. 3. Variation of the effective capture radius vs the defect size.

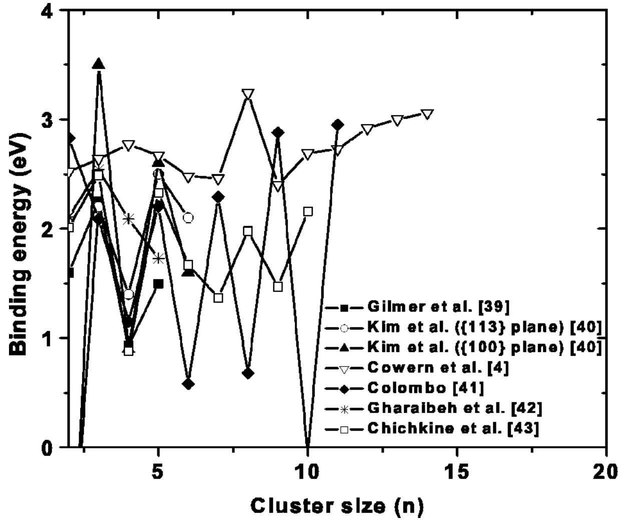

FIG. 4. Binding energy of a Si atom as a function of the cluster size as reported in the literature.

formation energies of the extended defects have to be accurately determined to allow a predictive estimation of transient diffusion effects. As for the calculation of the effective capture radius of defects and as it was suggested in recent investigations,[5,24] we will distinguish between small interstitial clusters ($n<10$) and elongated {113} defects ($n\geqslant 10$) to calculate their differential formation energies.

H. Small compact clusters: $n<10$

As we said in a previous section, little is known experimentally about the structure of small self-interstitial clusters in silicon and the absolute values of their binding energies—differential formation energies—are still not well determined. However, recent experimental[4] and theoretical[39–43] investigations all strongly suggest the presence of maxima in the binding energy curve. They were called "magic sizes" because of the enhanced stability of the corresponding clusters. However, the amplitudes and positions of these maxima are still under debate, as shown in Fig. 4. The data attributed to Cowern *et al.*[4] were derived by assuming a formation energy of 3.8 eV for self-interstitials. The discrepancies observed in the calculations of binding energies of self-interstitial clusters are mainly due to the large cell sizes that are needed to allow the relaxation of large clusters. A further problem is certainly to find the minimum-energy configuration for each self-interstitial cluster. Therefore, we will consider the differential formation energies of the small clusters, i.e., $E^f(2)$ to $E^f(9)$, as free parameters of our model.

I. {113} defects

Considering the simple structure of {113} defects, it is possible to approximate their formation energies by an analytical expression. First, we can reasonably assume that the vibrational entropy associated with a defect of n atoms is largely the same as that of a defect of $n+1$ atoms. Then, if we neglect the change in volume of the system during the dissociation $I_{n+1}\rightarrow I_n+I$, the differential formation energy $E^f(n+1)=G^f_{I_{n+1}}-G^f_{I_n}$ simply reduces to $U_{I_{n+1}}-U_{I_n}$, i.e., the increase in internal energy when adding one single host atom to a defect of n atoms. The internal energy of a {113} defect is composed of the fault energy and the elastic energy,[44] which can be calculated in the framework of the theory of dislocations in isotropic continua. It is thus possible to calculate the differential formation energy of {113} defects from their crystallographic characteristics. As shown by Hull and Bacon,[45] the two edge dislocations plus the two mixed dislocations define the strain energy of a {113} defect, given by the following expression:

$$E_{strain}(n)=\frac{\mu b^2 L}{2\pi(1-\nu)}\ln\left(\frac{2W}{b}\right)+\frac{\mu b^2 W}{2\pi}\left\{\cos^2\theta+\left(\frac{\sin^2\theta}{1-\nu}\right)\right\}\ln\left(\frac{2L}{b}\right). \quad (13)$$

where μ denotes the shear modulus of silicon (μ=7.55 $\times 10^{10}$ N/m^2), ν the Poisson ratio (ν=0.3), b the length of the Burgers vector—considered as a free parameter—, and θ is the angle between the Burgers vector[32] and the normal vector perpendicular to the plane of the defect (θ=77.8°). As in Eq. (12), L and W stand for the length and the width of the defect, respectively.

Adding the contribution of the stacking fault to the strain energy, one finally obtains the self-energy U_{I_n} of a {113} defect containing n atoms:

$$U_{I_n}=E_{strain}(n)+\gamma n. \quad (14)$$

Here, γ is the stacking-fault energy per atom and considered as a free parameter of our model. Then, the differential formation energy of a {113} defect of n atoms is simply given by the difference $U_{I_{n+1}}-U_{I_n}$, or by dU_{I_n}/dn, when n can be considered as a continuous variable, i.e., when the size of the defect is large. Since the areal density of {113} defects is known and since they have a constant width (4 nm), the length and the width of the defect are related to the number of atoms n by the following relation:

$$n=(5\times 10^{14}\ \mathrm{cm}^{-2})WL=(20/\mathrm{nm})L. \quad (15)$$

IV. EXTRACTION OF PARAMETERS FROM EXPERIMENTS

In the preceding section we have defined two important characteristics of the extended defects: the effective capture radius and the differential formation energy. The former reflects their geometry and their ability to capture interstitials while the latter reflects their energetic properties, in other words, their stability. However, some parameters of the model are unknown, such as the differential formation energies of small clusters, or are not well determined, such as the Burgers vector of {113} defects. Hence these free parameters of the model must be either calculated, e.g., by first-principle calculations, or extracted from experimental data. The free parameters of our model are the following: $E^f(2)$ to $E^f(9)$, the differential formation energies of small interstitial clusters; γ, the stacking fault energy per atom of {113} defects; b, the Burgers vector of {113} defects; $D_I(T)$, the diffusion

coefficient of self-interstitials at temperature T; and C_I^{eq}, the equilibrium concentration of self-interstitials at temperature T.

Unfortunately, for the reasons we mentioned in a previous section, results obtained from calculations can sometimes be contradictory, as shown in Fig. 4. Therefore, the free physical parameters of our model were not calculated but extracted from experimental data. The data we use in this work were obtained from dedicated experiments in which a near-surface silicon implantation is used to generate a large amount of self-interstitials. During thermal annealings, they agglomerate into extended defects—small silicon clusters and {113} defects in our case—the thermal evolution of which can be investigated by different characterization techniques. For instance, their size distribution and/or density can be determined by transmission electron microscopy while the interstitial supersaturation they maintain in their vicinity is usually monitored via the diffusion of buried boron marker layers.[4,46] It has to be noted that in such experiments—carried out at relatively high temperature—the supersaturation quickly reaches a quasisteady state and only the transport capacity of self-interstitials, i.e., the product $D_I C_I^{eq}$, can be determined. Preliminary simulations were consistent with this concept and showed to be sensitive only to the product $D_I C_I^{eq}$ rather than to one of the individual parameters.

In this work, different types of experimental data, obtained under different experimental conditions, were combined in the same optimization strategy. On one hand, we used the evolution of the self-interstitial oversaturation measured by Cowern *et al.*[4] on samples annealed at 600 and 800 °C in a N_2 ambient after implantation of Si^+ with 40 keV and a dose of 2×10^{13} cm^{-2}. On the other hand, the mean-size evolution of {113} defects obtained by TEM analysis[17] was also included in the fitting procedure. These TEM measurements were carried out on samples implanted with Si^+ at 40 keV and a dose of 6×10^{13} cm^{-2}, annealed at 740 °C in N_2 ambient for different times. It is important to note that the combination of self-interstitial oversaturation and TEM data was necessary to eliminate unphysical solutions and find the optimum set of physical parameters. Indeed, preliminary optimization of parameters performed on only oversaturation data showed that the resulting calibrated model could account for the evolution of the self-interstitial oversaturation at different temperatures but was not able to reproduce TEM observations.

However, extraction of parameters is not always an easy task and can be CPU-time consuming, especially when several parameters have to be extracted at the same time from the measured data. For instance, traditional optimization search algorithms using gradients have the disadvantage of getting "trapped" in local minima and, hence, require good estimates for the starting values for the physical parameters, which is sometimes impossible (see example given in Fig. 4). On the other hand, random-search methods do not require gradient calculations, but being a blind search they tend to be slow. Genetic algorithms (GAs), exceptional tools offered by artificial intelligence techniques, represent an interesting alternative. Based on the evolutionary ideas of natural selection and genetics,[47] GAs are designed to simulate processes in natural systems, especially those that follow the principles first laid down by Charles Darwin of survival of the fittest. As such, they represent an intelligent exploitation of a random search within a defined search space to solve a problem. To find the optimum solution to a given problem, GAs employ a population of individuals, each individual representing the set of parameters to be optimized. Using concepts of genetics, each individual—solution—is encoded as a binary string where a bit is analogous to a gene and a string is analogous to a chromosome. A population of individuals is then initialized at random and evolves to the next generation by genetic operators such as selection, crossover, and mutation. A fitness function is used to evaluate solutions and to represent the abilities of an individual to "compete." Consequently, genes from "good" individuals propagate throughout the population so that two good parents will sometimes produce offsprings that are better than their parents. Individuals in the population die and are replaced by the new solutions. In this way it is hoped that better solutions will thrive while the least fit solutions will die out. GAs have shown to be robust search algorithms and have already been successfully applied to wide variety of applications.[48–50] Therefore, we based our optimization strategy on a GA which was implemented by Fühner.[51] For our purpose, we used a population composed of 75 individuals and a restricted tournament operator for the selection of individuals, which is known to allow for a small population size while keeping a high diversity between individuals.[50] Although a high diversity level is already ensured by the use of a restricted tournament, we additionally introduced a low mutation rate of 0.001 to avoid any genetic drift,[52] i.e., to inhibit premature convergence to a local minimum in the search space.

Figure 5(a) shows the comparison between the interstitial supersaturation determined experimentally at 600 and 800 °C and our simulations after optimization of the parameters. As one can see, an excellent fit to the experimental data was obtained at both temperatures. Clearly, at 600 °C, the model is able to reproduce the different phases of evolution of the supersaturation, more precisely, the ultrafast TED phase followed by the sharp drop in supersaturation and the lower "plateau" with an almost constant supersaturation of about 10^4. Our model also reproduces very well the fact that ultrafast TED phase is not observable anymore after 1 s annealing at 800 °C. Furthermore, the time at which the system returns to equilibrium, i.e., the steep drop of the supersaturation to low values around 100 s, is perfectly accounted for by the model at this temperature. This steep drop of the supersaturation is of course attributed to the final dissolution of the extended defects. The comparison between the measured mean length of the {113} defects at 740 °C and the simulation after optimization is shown in Fig. 5(b). Taking into account uncertainties that are inherent to a quantitative TEM analysis, a very good agreement is obtained.

V. DISCUSSION AND VALIDATION

The values we extracted for the differential formation energies of small self-interstitial clusters and {113} defects

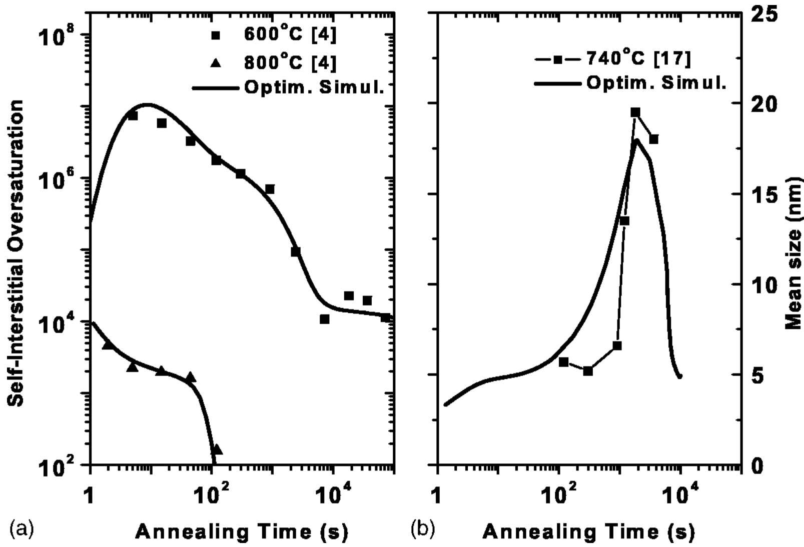

FIG. 5. Comparison between experimental data used during extraction of parameters and simulation after optimization: (a) oversaturation evolution, (b) evolution of the mean length of {113} defects.

are presented in Table I and plotted in Fig. 6. At the first sight, we can see that the differential formation energies of small clusters ($n < 10$) exhibit two strong minima at $n = 4$ and $n = 8$. This means that clusters containing four or eight atoms are particularly stable. Other investigations, experimental as well as theoretical ones, also predicted the existence of a nonmonotonic trend in the binding energy curve, as shown in Fig. 4. This strongly suggests that the presence of the two minima we found is not an artifact of the extraction of parameters but represents real physics. Actually, the presence of oscillations is not so surprising. Indeed, it is very plausible that for certain sizes, the capture of an extra interstitial by a small cluster considerably modifies the stress that the cluster exerts on its surrounding and requires a lattice relaxation, leading to a reduction of the energy of the system. Furthermore, our model would completely fail to fit the data at 600 °C if we applied the constraint that the differential formation energy varies monotonically. As it was shown by Ortiz and Mathiot,[8] with this constraint, the oversaturation varies smoothly in time, in contrast to the sharp drop seen after 10^3 s at 600 °C. Thus, at low temperature, the evolution of the self-interstitial oversaturation at the beginning of the annealing is determined by the differential formation energies of stable clusters that act as a statistical energy barrier against the growth towards larger defects. Then, during the period $10^3 - 10^4$ s, defects undergo a fast structural transition from small self-interstitial clusters to {113} defects, which corresponds to the sharp drop in the oversaturation, as shown in Fig. 5(a). The values found by Cowern *et al.*[4] for the differential formation energies of small clusters are also reported in Fig. 6 for comparison. It is interesting to note that, although the authors used a zero-dimensional model with a partially different physics and although they extracted different absolute values, the positions of minima are the same, i.e., at sizes 4 and 8. It has to be emphasized at this point that the initial conditions for the GA as well as the optimization strategy were unbiased so that the particular positions of the minima were by no means predetermined.

TABLE I. Optimized values for the differential formation energies of small self-interstitial clusters.

Number of atoms	2	3	4	5	6	7	8	9
(eV)	1.67	1.34	0.95	1.4	1.49	1.23	0.94	1.17

For the {113} defects, i.e., for sizes of 10 and beyond, we found a stacking-fault energy per atom of 0.38 eV, close to the lower limit estimated by *ab initio* calculations.[32] A value of 1.1 Å was obtained for the Burgers vector b of the {113} defects. This value is in very good agreement with HRTEM observations which estimate b to range from $0.032a\langle 116\rangle = 1.07$ Å to $a/25\langle 116\rangle = 1.34$ Å. Adding the contributions of the strain and stacking-fault energies, we find the asymptotical differential formation energy of very large {113} defects to be about 0.7 eV, in very good agreement with values obtained in other investigations.[30,53,54] In Fig. 7 we reported the different values for the transport capacity of self-interstitials in silicon extracted with the GA as a function of temperature. As evidenced, the temperature dependence of the self-diffusivity follows an Arrhenius law. Our values are close to those found by Cowern *et al.*[4] in the same temperature range and are also in good agreement with

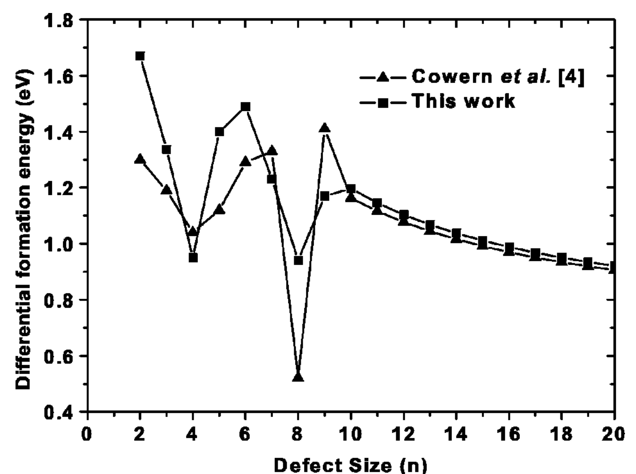

FIG. 6. Differential formation energies of defects extracted by GA optimization (squares) and from Cowern *et al.* (triangles).

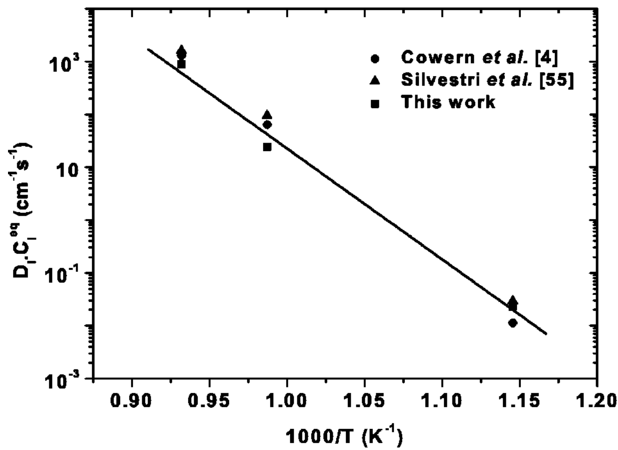

FIG. 7. Transport capacity of self-interstitials extracted by GA optimization (squares), from Cowern *et al.* (circles) and from Silvestri *et al.* (triangles).

a recent self-diffusion experiment reported by Silvestri *et al.* [55]

In order to test the validity of our physically based model as well as the consistency of the extracted parameters, the calibrated model was used to simulate various types of experimental data found in complementary investigations.[2,4,11,17]

A. Self-interstitial oversaturation and mean-size evolution

As a first test, we used our calibrated model to reproduce similar data as those used in the optimization routine, namely, the self-interstitial oversaturation and mean size of defects. To do so, we used complementary oversaturation data. One data set was obtained by Cowern *et al.*[4] on samples implanted with Si^+ ions at 40 keV for a dose of 2×10^{13} cm^{-2} and annealed at 700 °C under a N_2 ambient. The other one was measured by Cristiano *et al.*[17] on samples implanted Si at 40 keV for a dose of 6×10^{13} cm^{-2} and annealed at 740 °C under N_2. Finally, we used the TEM data of Eaglesham *et al.*[2] measured on samples annealed at 815 °C for different times after a Si implantation at 40 keV for a dose of 5×10^{13} cm^{-2} as an independent test for the mean-size prediction. Results of simulations on the oversaturation evolution are reported in Fig. 8(a) and compared to experimental data. Clearly, the model predicts very well the time dependence of the self-interstitial oversaturation maintained by the extended defects. The results obtained on the mean-size evolution of defects at a temperature of 815 °C are presented in Fig. 8(b). As we can see, the TEM data are well reproduced by the model, considering the inherent uncertainties of TEM analysis.

B. Dissolution of {113} defects during TED

For a second validation test, we used our calibrated model to simulate TEM observations on the time evolution of the number of Si atoms stored in {113} defects. For comparison, TEM data obtained in two independent experiments were used. In the first one, carried out by Eaglesham *et al.*,[2] samples were implanted with Si^+ ions at 40 keV for a dose of 6×10^{13} cm^{-2} and annealed under various conditions. The second set of experimental results we used was recently obtained by Cristiano *et al.*.[17] Therein, Si^+ ions were implanted with 40 keV and a dose of 6×10^{13} cm^{-2} prior to annealing at different temperatures for different times. Figure 9 shows a comparison between simulations with the calibrated model and the TEM data mentioned. All simulations were performed by keeping the optimized parameters, except the product $D_I C_I^{eq}$, constant. The latter was adjusted for each temperature. In each case, the value used for the product $D_I C_I^{eq}$ and giving the best fit to the data was in good agreement with the values obtained during the optimization of parameters and with values found in the literature.[4,55] Clearly, the model is able to reproduce the dissolution of {113} defects over a broad range of temperatures. The model shows that a maximum of about 80% of the interstitials initially created by the Si implantation are trapped in extended defects. The other 20% have either recombined at the surface or diffused into the bulk. This is in good agreement with experimental observations. In addition, the model predicts that at low annealing temperatures—650 and 670 °C—the number of interstitials in extended defects first increases be-

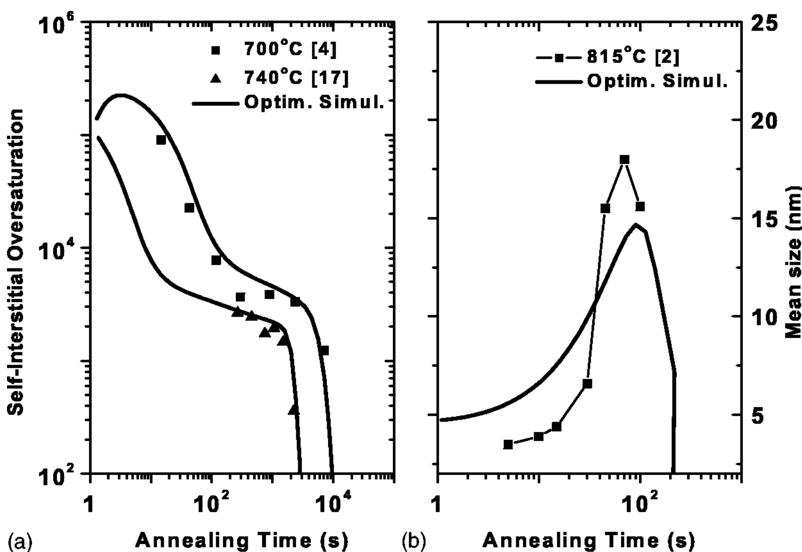

FIG. 8. Comparison between experimental data and simulation with the optimized set of parameters: (a) oversaturation evolution, (b) evolution of the mean length of {113} defects.

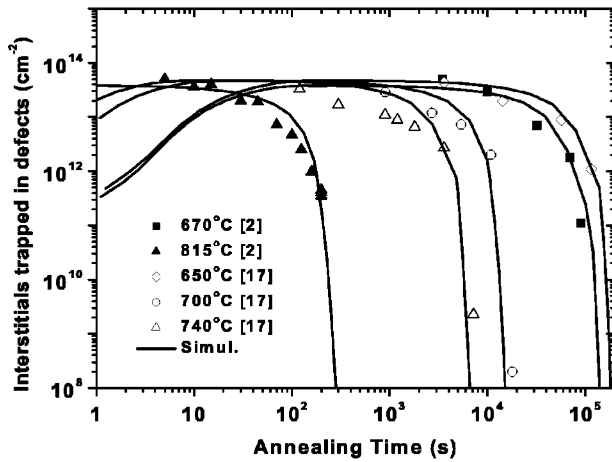

FIG. 9. Comparison between measured trapped interstitial dose at various temperatures and simulations with the optimized parameter set.

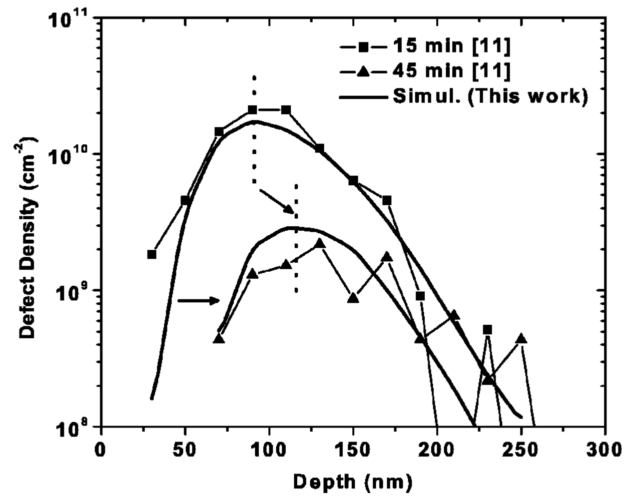

FIG. 11. Comparison between measured depth distribution of defects and simulations with the optimized set of parameters at 740 °C for 15 and 45 min annealing.

fore it reaches an almost constant value. This increase is only apparent, as we shall demonstrate in the following. In fact, almost all interstitials are already trapped in defects at the very beginning of the annealing, although they are all not observable. This is illustrated in Fig. 10 that shows the contributions of small compact clusters and {113} defects to the trapped interstitial dose. The simulations reported in this figure were performed assuming an initial Si implantation dose of 5×10^{13} cm^{-2} and a temperature of 670 °C, i.e., one of the conditions of Eaglesham's experiment. The figure clearly shows that after 1 s annealing, almost all interstitials that were created during implantation are already bound to defects (squares). However about 80% of the interstitials are in small compact clusters (circles) and the rest can be found in small {113} defects (triangles). Both types of defects are smaller than 2 nm so that neither is accessible to TEM investigations. Therefore, at the beginning of the annealing, only a small fraction of the trapped dose is experimentally observable (solid line). For longer annealing times, between 1 and 300 s, small clusters transform into {113} defects, which at the same time grow and become observable by TEM. This explains the apparent increase in the trapped interstitial dose. Then, {113} defects evolve following a classical Ostwald ripening process, during which a weak interstitial loss from the defect band is observed. Typically, during this regime, defects increase in size while their density decreases.[36] After 10^4 s of annealing at 670 °C, defect dissolution occurs rapidly and the dose of interstitials trapped in defects drops abruptly. As it has already been reported in several investigations, the dissolution of {113} defects is due to the flux of self-interstitials from the defect layer toward the surface, which is known to be a strong sink for point defects.

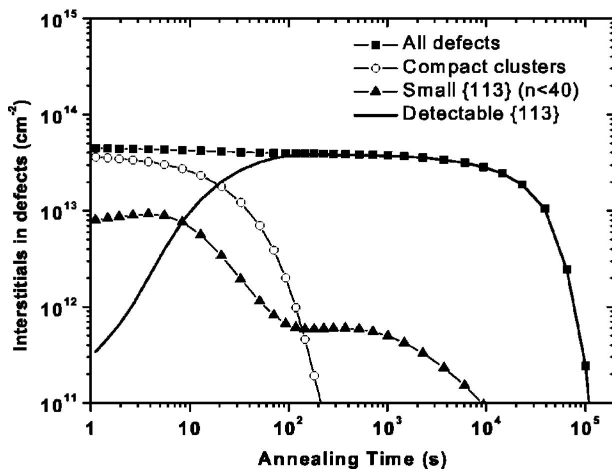

FIG. 10. Time evolution of the trapped interstitial dose contained in all defects (squares), compact clusters (circles), small {113} defects (triangles), and detectable {113} defects (solid line).

C. Time evolution of the depth distribution of {113} defects

As it was mentioned previously, the surface plays a major role in the dissolution of defects. During annealing, the surface acts as an efficient sink for point defects and consequently, a flux of self-interstitials from the defect layer to the surface is established. This leads to the notion that the defect band should dissolve preferentially on the near-surface side, leading to an increase in mean depth of the band with time. Recently, Colombeau *et al.*[11] studied the time evolution of the depth profile of {113} defects experimentally in order to resolve this issue. Briefly, in this experiment, samples were Si^+ implanted at 40 keV for a dose of 6×10^{13} cm^{-2} and annealed for various times at a temperature of 740 °C. After processing, the authors measured the density of defects as a function of depth by means of quantitative TEM analysis. This experiment clearly demonstrated for the first time the preferential dissolution of the defect band on the near-surface side. Their experimental results provide thus a critical test to our model. In order to reproduce this experiment and to test the ability of our model to predict the spatial evolution of the defect band, we simulated the formation of extended defects at a temperature of 740 °C for annealing times of 15 and 45 min. In Fig. 11, our simulations are compared to the depth distributions of defects measured by Colombeau *et al.*[11] Clearly, the agreement is very good and our model predicts not only the spatial extension of the defect band but also the

overall density decrease due to the Ostwald ripening of the defects. Finally, Fig. 11 clearly demonstrates that our model reproduces very well the observed asymmetric dissolution of the defect band, which is a consequence of the vicinity of the surface at which self-interstitials may recombine effectively.

VI. CONCLUSION

In this paper we have presented a physically based model implemented one dimensionally that accounts for nucleation, growth, and dissolution of extended defects in ion-implanted silicon. The model describes the diffusion of self-interstitials, their agglomeration, as well as their recombination at the silicon surface. The rates at which self-interstitials attach/dissociate to/from extended defects were derived on the basis of kinetic and thermodynamic considerations. We have introduced two parameters, the effective capture radius and the differential formation energy of the extended defects, which determine the capture and emission rate constants. Both parameters will depend on size and geometry of the extended defects and were given for the particular case of small compact silicon clusters and for elongated $\{113\}$ defects. The pertinent physical parameters of the model were presented and determined from self-interstitial oversaturation and TEM measurements by means of a genetic algorithm. We have found that the differential formation energy of small compact clusters exhibits two strong minima, as previously reported in other investigations. The other parameters are in good agreement with values found in the literature. We have demonstrated that our calibrated model is able to reproduce a variety of experimental observations with good agreement and in a wide range of experimental conditions. This includes, for example, the evolution of the mean size of defects, the dissolution of $\{113\}$ defects, the time dependence of the self-interstitial oversaturation, and even the spatial evolution of the depth distribution of $\{113\}$ defects with annealing time.

ACKNOWLEDGMENT

Part of this work was carried out within FRENDTECH funded by the European Community as IST Project No. 2000-30129.

[1] C. Bonafos, M. Omri, B. de Mauduit, G. Ben Assayag, A. Claverie, D. Alquier, A. Martinez, and D. Mathiot, J. Appl. Phys. **82**, 2855 (1997).
[2] D. J. Eaglesham, P. A. Stolk, H.-J. Gossmann, and J. M. Poate, Appl. Phys. Lett. **65**, 2305 (1994).
[3] N. E. B. Cowern, G. F. A. van de Walle, P. C. Zalm, and D. W. E. Vandenhoudt, Appl. Phys. Lett. **65**, 2981 (1994).
[4] N. E. B. Cowern *et al.*, Phys. Rev. Lett. **82**, 4460 (1999).
[5] A. Claverie, B. Colombeau, F. Cristiano, A. Altibelli, and C. Bonafos, in *Si Front-End Processing-Physics Technology of Dopant-Defect Interactions III*, edited by M. A. Foad, J. Matsuo, P. Stolk, M. D. Giles, and K. S. Jones, Mater. Res. Soc. Symp. Proc. No. 669 (Materials Research Society, Pittsburgh, 2001), p. J9.4.1.
[6] A. H. Gencer and S. T. Dunham, J. Appl. Phys. **81**, 631 (1997).
[7] G. Hobler and C. S. Rafferty, in *Si Front-End Processing-Physics and Technology of Dopant-Defect Interactions*, edited by H-J. L. Gossmann, T. E. Haynes, M. E. Law, A. N. Larsen, and S. Odanaka, Mater. Res. Soc. Symp. Proc. No. 568 (Materials Research Society, Pittsburgh, 1999), p. 123.
[8] C. J. Ortiz and D. Mathiot, in *Si Front-End Processing-Physics and Technology of Dopant-Defect Interactions III*, edited by M. A. Foad, J. Matsuo, P. Stolk, M. D. Giles, and K. S. Jones, Mater. Res. Soc. Symp. Proc. No. 669 (Materials Research Society, Pittsburgh, (2001), p. J5.6.1.
[9] D. Turnbull and J. C. Fisher, J. Chem. Phys. **17**, 71 (1949).
[10] P. Hanggi, H. Grabert, P. Talkner, and H. Thomas, Phys. Rev. A **29**, 371 (1984).
[11] B. Colombeau, N. E. B. Cowern, F. Cristiano, P. Calvo, N. Cherkashin, Y. Lamrani, and A. Claverie, Appl. Phys. Lett. **83**, 1953 (2003).
[12] D. Lim, C. Rafferty, and F. Klemens, Appl. Phys. Lett. **67**, 2302 (1995).
[13] S. M. Hu, Appl. Phys. Lett. **27**, 165 (1974).
[14] S. M. Hu, Appl. Phys. Lett. **45**, 1567 (1974).
[15] N. E. B. Cowern, D. Alquier, M. Omri, A. Claverie, and A. Nejim, Nucl. Instrum. Methods Phys. Res. B **148**, 257 (1999).
[16] M. D. Giles, J. Electrochem. Soc. **138**, 1160 (1991).
[17] F. Cristiano *et al.*, Nucl. Instrum. Methods Phys. Res. B **216**, 46 (2004).
[18] J. P. Biersack and L. G. Haggmark, Nucl. Instrum. Methods **174**, 257 (1980).
[19] G. D. Watkins, *Radiation Damage in Semiconductors* (Dunot, Paris, France, 1964), pp. 97–113.
[20] V. A. Panteleev, S. N. Ershov, V. V. Chernyakhovskii, and S. N. Nabornykh, JETP Lett. **23**, 633 (1976).
[21] S. Coffa and S. Libertino, Appl. Phys. Lett. **73**, 3369 (1998).
[22] P. Pichler, W. Jungling, S. Selberherr, E. Guerrero, and H. W. Pötzl, IEEE Trans. Comput.-Aided Des. **4**, 384 (1985).
[23] F. Cristiano, B. Colombeau, N. E. B. Cowern, and A. Claverie (private communication).
[24] B. Colombeau, Ph.D. thesis, Université Toulouse III-Paul Sabatier, September, 2001.
[25] Philibert, *Diffusion et Transport de Matière dans Les Solides* (Les Editions de Physique, Les Ulis, 1991).
[26] T. R. Waite, Phys. Rev. **107**, 463 (1957).
[27] S. Takeda, in Proceedings of Microsc. Semicond. Mater. Conference, edited by A. G. Cullis and A. E. Stanton-Bevan (Institute of Physics, Bristol, 1997); Inst. Phys. Conf. Ser. **157**, 25 (1997).
[28] C. A. Ferreira Lima and A. Howie, Philos. Mag. **34**, 1057 (1976).
[29] I. G. Salisbury and M. H. Loretto, Philos. Mag. A **39**, 317 (1979).
[30] A. Claverie, B. Colombeau, B. de Mauduit, C. Bonafos, X. Hebras, G. Ben Assayag, and F. Cristiano, Appl. Phys. A: Mater. Sci. Process. **76**, 1025 (2003).
[31] F. Cristiano, B. Colombeau, and A. Claverie (private communication).
[32] S. Takeda, M. Kohyama, and K. Ibe, Philos. Mag. A **70**, 287 (1994).
[33] N. Cherkashin *et al.* (unpublished).
[34] M. M. De Souza, M. P. Chichkine, and E. M. Sankara Narayanan, in *Si Front-End Processing-Physics and Technology of Dopant-Defect Interactions III*, edited by A. Agarwal, L. Pelaz, H.-H. Vuong, P. Packan, and M. Kase, Mater. Res. Soc. Symp. Proc. No. 610 (Materials Research Society, Pittsburgh, 2000), p. B11.3.1.
[35] G. J. Ackland, Phys. Rev. B **55**, 16186 (1997).
[36] A. Claverie, B. Colombeau, F. Cristiano, A. Altibelli, and C. Bonafos, Nucl. Instrum. Methods Phys. Res. B **186**, 281 (2002).
[37] J. Li and K. S. Jones, Appl. Phys. Lett. **73**, 3748 (1998).
[38] P. Calvo, A. Claverie, N. Cherkashin, B. Colombeau, Y. Lamrani, B. De Mauduit, and F. Cristiano, Nucl. Instrum. Methods Phys. Res. B **216**, 173 (2004).
[39] G. H. Gilmer, T. Diaz de la Rubia, D. M. Stock, and M. Jaraiz, Nucl. Instrum. Methods Phys. Res. B **102**, 247 (1995).
[40] J. Kim, J. W. Wilkins, F. S. Khan, and A. Canning, Phys. Rev. B **40**, 10351 (1989).
[41] L. Colombo, *20th International Conference on Defects in Semiconductors*, edited by C. Van de Walle and W. Walukiewicz [Physica B 273-274, 458 (1999)].
[42] M. Gharaibeh, S. K. Estreicher, and P. A. Fedders, *20th International Conference on Defects in Semiconductors*, [Physica B 273-274, 532 (1999)].
[43] M. P. Chichkine, M. M. De Souza, and E. M. Sankara Narayanan, Phys. Rev. Lett. **88**, 085501 (2002).
[44] A. Parisini and A. Bourret, Philos. Mag. A **67**, 605 (1993).
[45] D. Hull and D. J. Bacon, *Introduction to Dislocations* (Pergamon, Oxford, 1984), p. 79.
[46] Y. Lamrani, F. Cristiano, B. Colombeau, E. Scheid, P. Calvo, H. Schäfer, and A. Claverie, Nucl. Instrum. Methods Phys. Res. B **216**, 281 (2004).
[47] J. H. Holland, *Adaptation in Natural and Artificial Systems* (The University of Michigan Press, Ann Arbor, 1975).
[48] D. M. Deaven and K. M. Ho, Phys. Rev. Lett. **75**, 288 (1995).
[49] M. Jaraiz, P. Castrillo, R. Pinacho, L. Pelaz, J. Barbolla, G. H. Gilmer, and

C. S. Rafferty, in *Si Front-End Processing-Physics and Technology of Dopant-Defect Interactions III*, edited by A. Agarwal, L. Pelaz, H.-H. Vuong, P. Packan, and M. Kase, Mater. Res. Soc. Symp. Proc. No. 610 (Materials Research Society, Pittsburgh, 2001), p. B11.1.1.
[50] T. Führer and T. Jung, J. Cryst. Growth **266**, 229 (2004).
[51] T. Führer, A. Erdmann, R. Farkas, B. Tollkühn, and G. Kókai, *Evo Workshops*, edited by In Raidl *et al.* (Springer, Berlin, 2004), pp. 208–218.
[52] D. E. Goldberg, *Genetic Algorithms in Search, Optimization and Machine Learning* (Addison-Wesley, Reading, MA, 1989).
[53] J. Kim, F. Kirchhoff, J. W. Wilkins, and F. S. Khan, Phys. Rev. Lett. **84**, 503 (2000).
[54] P. A. Stolk *et al.*, J. Appl. Phys. **81**, 6031 (1997).
[55] H. H. Silvestri, I. D. Sharp, H. A. Bracht, S. P. Nicols, J. W. Beeman, J. Hansen, A. Nylandsted-Larsen, and E. E. Haller, in *Defect and Impurity Engineered Semiconductors and Devices III*, edited by S. Ashok, J. Chevallier, N. M. Johnsonn, B. L. Sopori, and H. Okushi, Mater. Res. Soc. Symp. Proc. No. 719 (Materials Research Society, Pittsburgh, 2002), p. F13.10.1.